NANO LETTERS

pubs.acs.org/NanoLett Letter

Room-Temperature Exciton Polaritons in Monolayer WS_2 Enabled by Plasmonic Bound States in the Continuum

Cai Luo, Wei Li, Jianmei Li,* Ziyi Fu, Nannan Hu, Zhixiang Yu, Wenyao Chang, Pinxu Li, Xin Huang, Baoli Liu, Yang Yang, Aizi Jin, Baogang Quan, Shibing Tian, Haifang Yang, Yang Guo,* and Changzhi Gu*

Cite This: *Nano Lett.* 2025, 25, 4361−4368 Read Online

ACCESS | Metrics & More | Article Recommendations | Supporting Information

ABSTRACT: Exciton polaritons formed by the strong coupling between excitons and photons have been extensively studied in transition metal disulfides (TMDs) for their potential to inherit ultralong radiation lifetime and remarkable nonlinearity. Many studies have achieved strong coupling at room temperature. However, the systems in these studies generally lack orderly characteristics and precise controllability, and their tunability also remains rather limited. Here, we demonstrate a plasmonic grating with a bound state in the continuum (BIC) as a highly tunable platform for generating exciton polaritons in monolayer WS_2 at room temperature. We characterized the polariton modes and determined an energy splitting of 93 meV. This validates strong coupling in our system. Our research offers a new approach for exploring exciton polaritons in 2D semiconductors, opening doors for room-temperature optoelectronic and quantum computing applications.

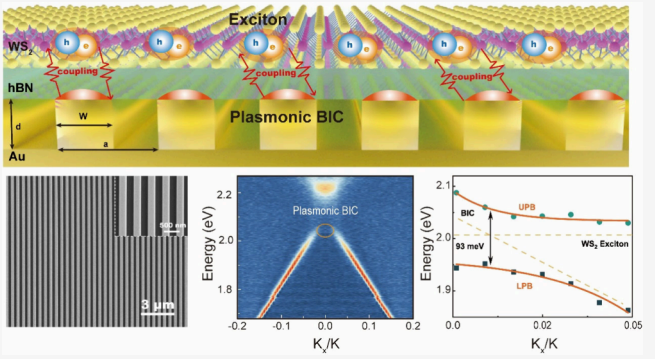

KEYWORDS: *plasmonic BIC, strong coupling, Rabi-splitting, exciton polariton*

Exciton polaritons, being hybrid quasiparticles with a half-light and half-matter nature, exhibit notably low effective masses and large nonlinearities.[1,2] These states enable for the observation of remarkable physical phenomena such as Bose−Einstein condensation[3] and superfluidity,[4] and also offer potential applications in low-threshold lasers[5] and quantum simulators.[6] In principle, exciton polaritons are generated through the strong coupling between excitons in semiconductors and photons confined in optical cavities.[7] Strong coupling occurs when the energy exchange rate between excitons and cavity photons surpasses both the exciton nonradiative relaxation rate and the cavity dissipation rate, which subsequently leads to vacuum Rabi splitting.[8,9] For the formation of exciton polaritons, optical cavity photons require a large quality (Q) factor and a small mode volume V_m. The Q factor is defined as the ratio of the resonant frequency ω to the loss γ. A large Q factor indicates a low photon loss rate in the cavity, which results in a longer lifetime of cavity photons and thus enhances the interaction time between excitons and photons.[10,11] The mode volume is related to the photon density. In an optical cavity, the photon density is inversely proportional to the mode volume V_m, such that a reduction of V_m leads to an elevation in photon density.[12−14] According to Fermi's golden rule, a higher density of final states enhances the transition rate between exciton and photon states, facilitating strong coupling and the formation of exciton polaritons.

Exciton polaritons have been extensively studied in several semiconductors, including GaAs,[15] TMDs,[16,17] and halide perovskites[18,19] over the years. Among these, TMDs are emerging as an ideal platform for achieving strong coupled exciton polaritons with a strong coupling. With a direct bandgap, TMDs are efficient light emitters. Their unique 2D layered structure enables a relatively large exciton binding energy, reaching up to several hundreds of meV,[17,20] due to strong confinement restricting the electron−hole motion and enhancing their interaction. Their large exciton binding energy facilitates stable exciton-polariton formation at room temperature,[20,21] while minimizing nonradiative relaxation pathways and inhomogeneous broadening.[22]

Various optical microcavities, such as Fabry−Perot (FP) cavities,[17,23] distributed Bragg reflectors (DBRs),[24,25] metal

Received: December 17, 2024
Revised: March 3, 2025
Accepted: March 4, 2025
Published: March 5, 2025

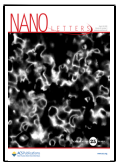

https://doi.org/10.1021/acs.nanolett.4c06464
Nano Lett. 2025, 25, 4361−4368

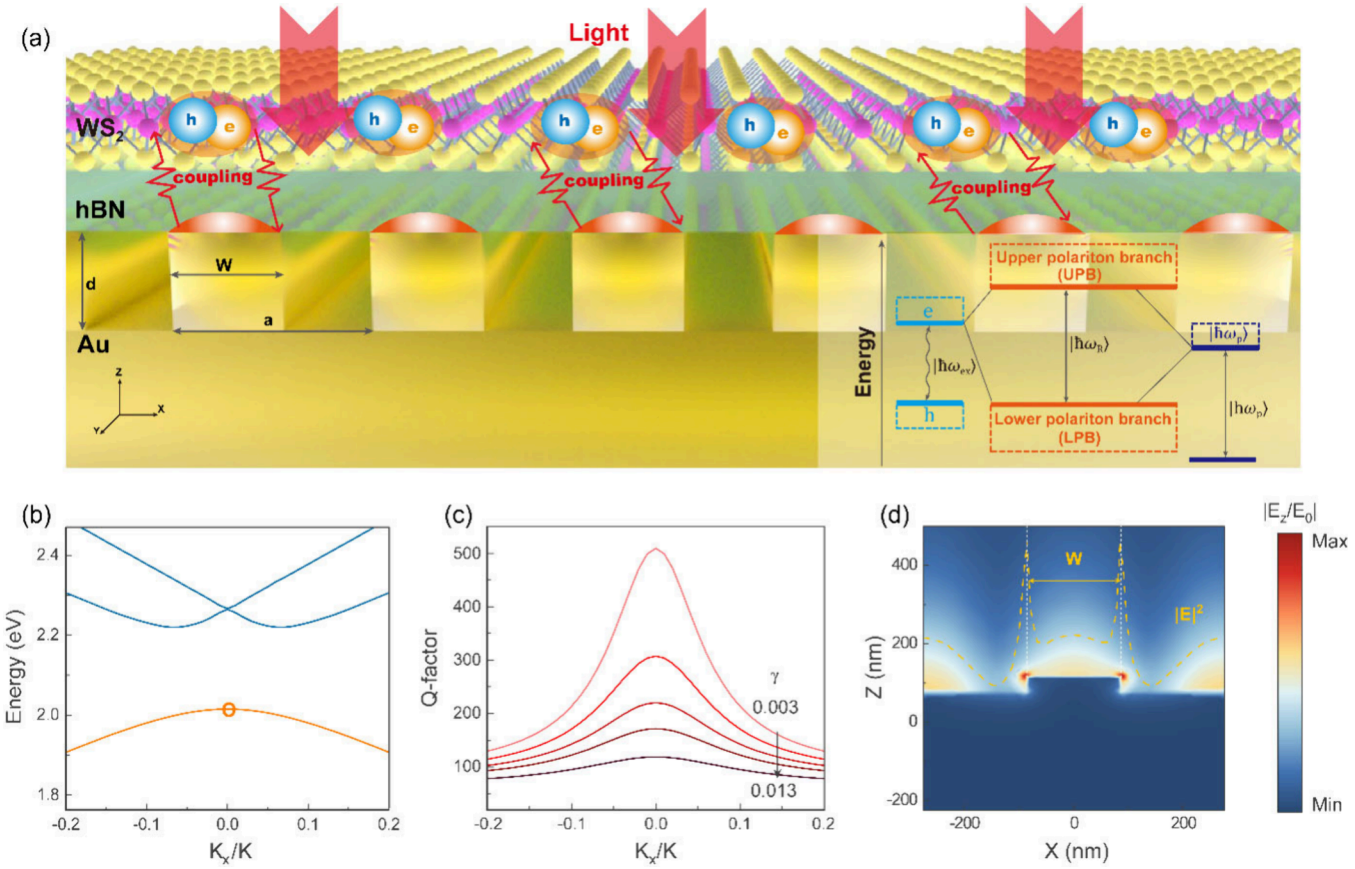

Figure 1. 1D grating platform supporting a plasmonic BIC for the formation of exciton polaritons in a monolayer WS_2 at room-temperature. (a) The schematic of the strong coupling between a plasmonic BIC and TMD excitons. The right panel depicts the energy diagram of the strong coupling of the WS_2 excitons with the energy of $\hbar\omega_{ex}$ coupled to the plasmonic BIC with the energy of $\hbar\omega_p$. The strong coupling forms hybrid states (UPB and LPB) separated by a Rabi splitting energy of $\hbar\omega_R$. (b) The band structure of the 1D grating. The at-Γ plasmonic BIC is marked with a circle. (c) Distribution of Q factors in momentum space as a function of loss coefficients (γ). (d) The calculated $|E_z/E_0|$ electric field distribution of the plasmonic BIC. The inset (dashed line) shows the profile of the square of the electric field along the *x*-axis.

nanoparticles,[26−28] plasmonic arrays,[29−32] and all-dielectric photonic crystal (PC),[33−35] have been explored for the formation of exciton polaritons in monolayer TMDs. Although FP cavities and DBRs are characterized by their large Q factors,[36,37] they are constrained in postprocessing capabilities. Due to the absence of mode-engineering design parameters, their cavity structures are bulky and rigid, thereby restricting their utility in more flexible and customizable experiments. Metal nanoparticles and plasmonic arrays exploit plasmonic modes to confine strong electric fields,[27,38−40] resulting in a small V_m that facilitate interaction with TMDs and enable a Rabi splitting in the range of 100−200 meV. Nevertheless, these structures based on metal nanoparticles suffer from some drawbacks, such as their random distribution, a lack of order and control, and limited tunability, making it difficult to precisely adjust their properties for practical applications. Moreover, due to the inherent losses of metal, they generally have low Q factors, which affects system performance. Compared to metal structures, all-dielectric PCs have cavity modes with a larger V_m, although these modes are localized within the dielectric.[41,42] When TMDs are placed on the dielectric surface, a spatial misalignment between excitons and cavity modes occurs, making it challenging for all-dielectric PCs to achieve large Rabi splitting energy at room temperature. Consequently, it is essential to develop optical microcavities that simultaneously possess a large Q factor, a small V_m, excellent tunability, and high compatibility with transition metal dichalcogenides (TMDs). It is essential to develop optical microcavities that simultaneously possess a large Q, a small mode volume (V_m), excellent tunability, and high compatibility with TMDs.

Here, we design a one-dimensional (1D) grating supporting a plasmonic BIC as a robust strong-coupling platform. The plasmonic BIC exhibits a high Q and a small mode volume (V_m), enabling the confinement of light within a smaller volume over an extended period and significantly enhancing the light-matter interaction. By utilizing the momentum-space imaging and PL measurements, we experimentally demonstrate a strong coupling between the plasmonic BIC and excitons of a monolayer WS_2. This coupling is characterized by the Rabi splitting of 93 meV at room temperature and is further corroborated by numerical simulations. Our results not only present novel design concepts regarding the strong coupling effect in 2D semiconductors but also offer new possibilities for exploring the collective behavior of exciton polaritons.

Figure 1(a) schematically depicts a 1D grating platform that supports a plasmonic BIC for strong coupling with excitons in a monolayer WS_2. The 1D grating is composed of parallel gold stripes on a Si substrate, with a thin gold film functioning as a mirror. By varying the stripe width (W) and the period (a) of 1D grating, the resonance frequency of the plasmonic BIC can be precisely tuned to match the exciton energy of WS_2. The

https://doi.org/10.1021/acs.nanolett.4c06464
Nano Lett. 2025, 25, 4361−4368

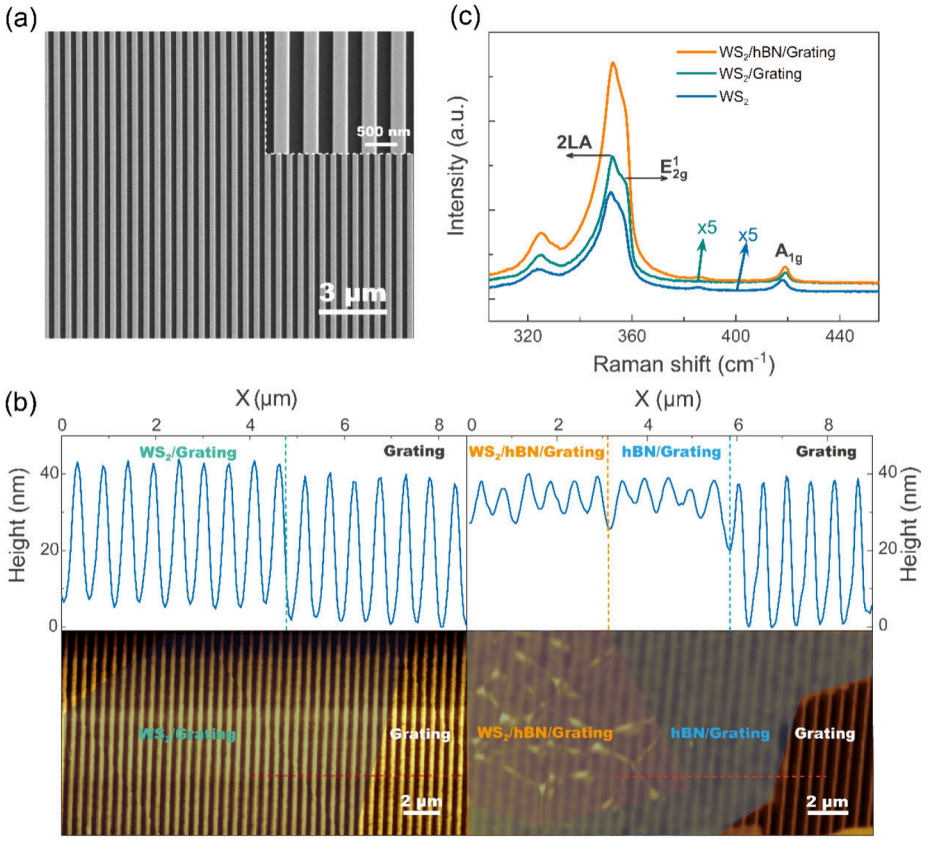

Figure 2. Characterization of the samples. (a) The SEM image of a 1D grating structure fabricated. The inset in the upper right corner is an enlarged image. (b) Atomic force microscopy (AFM) measurements of different heterostructures. The bottom row presents the corresponding AFM images, and the top row displays the height difference profiles of these heterostructures along the red line in the AFM images. (c) Raman spectra obtained from various heterostructures. All spectra were obtained under the same experimental conditions.

out-of-plane direction of the 1D grating is defined as the z-axis, while the in-plane direction across the gold stripes is defined as the x-axis. Figure 1b illustrates the band structure of the 1D grating in the momentum space, which is calculated by using the Quasinormal Modes (QNMs, see Supporting Information for details). For the sake of simplicity, only the transverse magnetic (TM) mode supporting a plasmonic BIC at Γ point is highlighted in orange.[43] The Q factor provides crucial information for identifying the TM mode as a plasmonic BIC. As shown in Figure 1c, the Q factor distribution in the momentum space indicates a peak of around 500 at the Γ point when the γ is 0.003, followed by a sharp decline with the increase of the wave vector K_x. γ is defined as the normalized metal loss factor $\gamma = \gamma_p/\omega_p$, where ω_p is the bulk equipartition excitation frequency and γ_p is the metal loss factor of Lorentz–Drude model. This behavior is consistent with the characteristic feature of at-Γ symmetry-protected BICs.[11] In addition, the Q factor of the plasmonic BIC is strongly dependent on γ, specifically, it becomes decreased by an order of magnitude when γ increases to 0.013. Moreover, the mirror symmetry of the electric field $|E_z/E_0|$ of the plasmonic BIC, as illustrated in Figure 1d, also indicates the characteristic constraint of the BIC.[44] The high Q factor and mirror symmetry provide compelling evidence for the BIC in this system. Finally, the plasmonic BIC has the ability to localize the light field within a small V_m on the surface of the grating,[45] characterized by the hot spots and an orange dashed line in Figure 1d. In addition, due to the in-plane orientation of the TMD exciton transition dipole moment, it shows a stronger correlation with the XY component of the electric field.[20] As shown in Supporting Information Note 2, the in-plane E_x/E_0 distribution exhibits pronounced localization patterns aligned with the TMD exciton dipole orientation, which critically enhances the coupling strength by maximizing spatial overlap between the plasmonic near-field and excitonic states. The combination of this small V_m and the high Q factor is highly favorable for the spatial coincidence of the plasmonic BIC and the WS_2 exciton resonance, which is essential for achieving strong coupling at room temperature in this study.

In our experiments, the 1D grating was fabricated using standard microfabrication techniques (see Supporting Information for details). Subsequently, it was characterized using a scanning electron microscope (SEM), as presented in Figure 2a. A monolayer of WS_2 was transferred onto the 1D grating with a hexagonal boron nitride (hBN) spacer. It is worth noting that the hBN spacer plays four crucial roles: preventing WS_2 degradation, avoiding short-range interactions (specifically charge transfer), reducing strain on the monolayer WS_2, and providing tunability of the BIC through its thickness.

Figure 2b displays the AFM images of WS_2 on the 1D grating with and without an hBN isolation layer. In the absence of the hBN isolation layer, the AFM image of WS_2 shows a periodic up-and-down morphology, with the height difference similar to that observed on the 1D grating. This suggests a strong influence of the underlying 1D grating structure on WS_2, with the periodic pattern of the 1D grating being transferred to the WS_2 layer, resulting in significant height variations. Conversely, in the presence of an hBN isolation

https://doi.org/10.1021/acs.nanolett.4c06464
Nano Lett. 2025, 25, 4361−4368

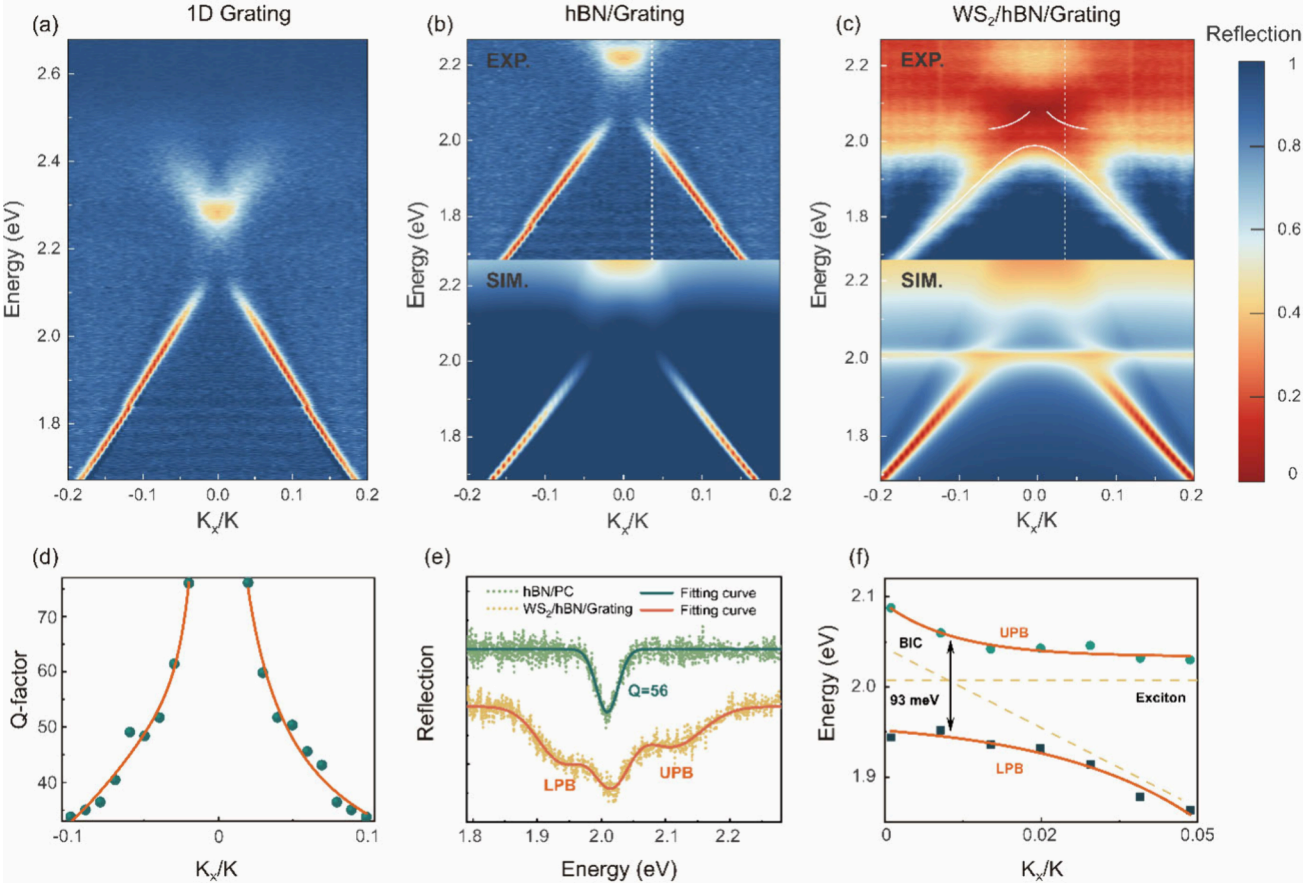

Figure 3. Demonstration of strong coupling between WS_2 excitons and plasmonic BIC modes in our sample. (a) The experimental momentum-space imaging of the bare 1D grating. (b,c) The experimental (top) and simulated (bottom) momentum-space imaging of the heterostructures of hBN/Grating and WS_2/hBN/Grating. The strong coupling is evidenced by the anticrossing phenomenon in (c). The solid lines refer to the polaritons resulting from strong coupling. (d) The typical Q-factor of plasmonic BICs extracted from the experimental measurement results. (e) The experimental reflectance spectra of hBN/Grating (olive line) and hybrid monolayer WS_2/hBN/Grating (orange line) correspond to the white dotted line ($K_x/K = 0.04$) in (b,c). (f) Dispersion relationship of exciton−plasmon polariton for the UPB and LPB fitted by the coupled-oscillator model.

layer, the AFM image of WS_2 exhibits much smaller undulations. The hBN layer likely acts as a buffer, reducing the direct influence of the 1D grating on the WS_2 layer, which results in a more uniform WS_2 layer with a minor height fluctuation.

Furthermore, Raman spectra were also utilized to evaluate the effect of the hBN isolation layer. As depicted in Figure 2c, the presence or absence of an hBN isolation layer significantly affects the Raman spectra of WS_2 on gratings, for example typical first-order modes $E_{2g}{}^1$ and A_{1g}, and the second order longitudinal acoustic phonon (2LA).[46,47] In the absence of the hBN isolation layer, the Raman spectra of WS_2 show that the intensities of these resonance peaks on the substrate are a little higher than those on the 1D grating. In contrast, when an hBN isolation layer is present, the Raman spectra of WS_2 on the grating exhibit a remarkable enhancement in the resonance peaks. Several factors can account for this enhancement. First, the hBN layer functions as a high-quality dielectric medium, modifying the local electric field around the WS_2 layer enhancing the light-exciton interaction, thereby increasing the Raman scattering efficiency. Second, the hBN layer may well keep the crystalline quality of WS_2.[48] A more ordered crystal lattice promotes more efficient phonon-related scattering processes, which are fundamental to the Raman spectra. Consequently, the resonance peaks become more distinct. Finally, the hBN layer can play a role in reducing interface scattering and nonradiative recombination.[49] This reduction enables a greater number of excitons to participate in Raman-active processes, contributing to the enhancement of the resonance peaks.

To observe the strong coupling between the plasmonic BIC and excitons of WS_2 in our sample, we measure the photonic dispersion (Figure 3) at room temperature using our homemade reflected momentum-space imaging spectroscopy (or angle-resolved reflectance spectroscopy) system (see Supporting Information for details). For comparison, we present the dispersion relation of the 1D grating along the direction K_x with $K_y = 0$ in Figure 3a. The measured photonic dispersion of the 1D grating is highly consistent with the simulation band structure shown in Figure 1b. The TM mode dispersion is clearly observable and vanishes around a photon energy of 2.107 eV at the Γ point, which is a characteristic of at-Γ symmetry-protected BICs.[50] Adding a 10 nm-thick hBN spacer would not change the BIC characteristics of the TM mode. However, it induces a red shift of approximately 56 meV in the BIC, aligning it closely with the resonance of the neutral exciton in the monolayer WS_2 (Figure 3b). We extracted the Q factor-K_x curves of BIC as shown in Figure 3d. As K_x increases,

https://doi.org/10.1021/acs.nanolett.4c06464
Nano Lett. 2025, 25, 4361−4368

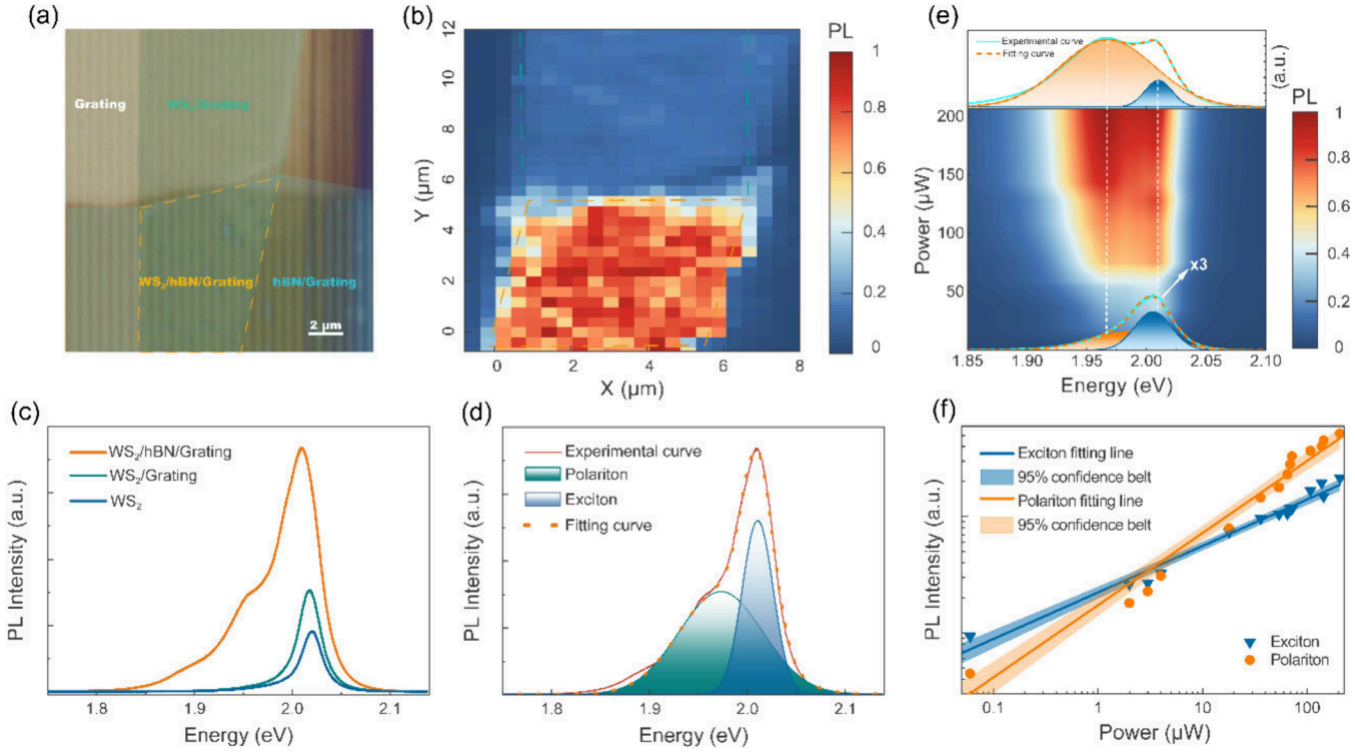

Figure 4. PL properties of WS_2-hBN-Grating. (a) Optical microscope image of our sample. The cyan and blue areas indicate the WS_2 and hBN coverage areas, respectively, and the orange dashed box shows their overlapping area (b) The PL intensity mapping image of A excitons of WS_2 in the range corresponding to (a). (c) PL spectra of the primitive WS_2 (blue), WS_2/grating (olive) and WS_2/hBN/grating (orange). (d) Experimental (orange solid line) and fitting (orange dotted line) PL spectra of the WS_2/hBN/grating at room temperature. Blue area and olive area below PL spectrum are contributions from two Gaussian fitting components. (e) Color map of the PL spectra as a function of pump powers at room temperature. The white dotted lines indicate the power-dependent exciton and polaritons energies. (f) Integrated PL intensities of both exciton and polariton with the pump power.

the Q factor gradually decreases, which is also one of the characteristics of at Γ BIC. Such reflection spectral evolution was further corroborated by numerical simulations (Figure 3b, bottom panel).

Figure 3c shows the momentum-space imaging of the 1D grating integrated with monolayer WS_2, which clearly shows the evolution process of strong coupling. The Rabi splitting can be clearly observed in our sample, which is manifested by the typical anticrossing dispersion of the lower-polariton branch (LPB) and upper-polariton branch (UPB). The experimental results closely align with simulations (Figure 3c, bottom panel), suggesting a strong coupling between the plasmonic BIC and excitons of WS_2. Figure 3e presents the reflection spectra extracted from the white dotted lines (K_x/K = 0.04) in Figure 3c (orange curve) and Figure 3b (olive curve) respectively, forming a strong contrast. The reflection spectrum after coupling has obvious Rabi splitting, where LPB and UPB can be clearly observed. To further confirm strong coupling, we fitted the extracted spectral positions of the UPB and LPB (E_{UPB} and E_{LPB}) with a coupled oscillator model[51] (see Supporting Information Note 5). The calculated polariton dispersions (orange curves) are in good agreement with our experimental data, as shown in Figure 3f. By fitting the reflection spectra, we extract a Rabi splitting of $\hbar\Omega_R = E_{UPB} - E_{LPB}$ = 93 meV, confirming the formation of exciton polaritons via strong coupling in our system.

To provide additional evidence of the exciton polaritons in this study, we performed micro-PL measurements on our sample. PL can provide a more direct evidence than reflectance spectra for distinguishing mode splitting from other effects such as enhanced absorption, plasma energy transfer, and Fano resonance, which helps to reveal and understand the underlying physical principles of resonant coupling.[26] A primitive monolayer WS_2 exhibits a strong A exciton emission (E_A = 2.013 eV) at room temperature, attributed to the direct optical transition at the K/K′ point in the Brillouin zone.[22] Figure 4b presents the PL intensity mapping of A excitons of WS_2, corresponding to the optical microscopy sample of Figure 4a. Due to strong coupling effect, the A exciton peak of WS_2 on hBN/Grating exhibits the highest intensity across the entire measured region. Compared to the primitive WS_2 monolayer, its enhancement factor is approximately 5-fold, while for the WS_2 on the grating without the hBN spacer, the enhancement is about 2-fold, as illustrated in Figure 4c. The difference of PL intensities can be attributed to the detuning between the plasmonic BIC mode and the exciton transition. In addition, the significant enhancement of the PL intensity of excitons also indicates that strong coupling can have a substantial impact on improving the quantum yield of WS_2.[52]

Importantly, an additional optical emission below A excitons was detected in the WS_2/hBN/grating. Through multipeak Gaussian fitting of the PL spectrum, as depicted in Figure 4d, the peak position of this newly observed PL peak was determined to be 1.973 eV. This peak coincides with the LPB identified in the reflectance spectrum, which strongly implies a robust coupling between the plasmonic BIC and the WS_2 excitons. At room temperature, no emission corresponding to the UPB observed in the reflection spectra was detected. This

https://doi.org/10.1021/acs.nanolett.4c06464
Nano Lett. 2025, 25, 4361−4368

can be attributed to thermal decomposition and phonon scattering processes.[29] Thermal decomposition may disrupt the necessary conditions for UPB emission, while phonon scattering cause energy dissipation, consequently suppressing the UPB-related emission.

Furthermore, we investigated the PL spectra at different powers. Figure 4e presents the 2D color map of PL spectra as a function of the pump power, range from 0.03 to 200 μW at room temperature. As the power increased, the PL intensities of both exciton and polariton exhibited a linear increase, with the polaritons presenting a more rapid rate of increase, as shown in Figure 4f. Beyond a certain power level (4 μW), the PL intensity of the LPB gradually becomes the dominant contributor. The absence of the polariton nonlinear phenomenon may be attributed to large metal-induced optical losses. In this system, the significant metal loss can lead to rapid relaxation of polaritons, impeding their interaction sufficiently to prevent nonlinear behavior.

In summary, we demonstrate 1D grating supporting BIC as a highly tunable and highly compatible platform for generating exciton polaritons in TMDs at room temperature, which is beneficial from its small mode volume and high Q factor. In detail, the exciton polaritons in a monolayer WS_2 have been confirmed through the measurement of their photonic dispersion in momentum space and Rabi splitting in both reflectance and PL spectra, indicating an anticrossing behavior with the energy splitting of 93 meV at room temperature. Both simulated and experimental results strongly validate the formation of exciton polaritons via strong coupling within our system. Our work not only offers a novel practical method for exploring exciton polaritons in 2D semiconductors but also paves new ways for studying new optoelectronic devices and the collective behavior relevant to quantum computing at room temperature.

Sample Fabrication. Ti layers of 5 nm and Au layers of 50 nm were deposited as mirrors on a commercial silicon substrate via electron beam evaporation. The grating was patterned on the mirror surface by a combination of electron-beam lithography and electron-beam evaporation, yielding the following geometrical parameters: pitch p = 480 nm, trench width w = 170 nm and depth d = 40 nm, as characterized by scanning electron and atomic force microscopy measurements. Large-area high quality flakes of multilayer hBN and monolayer WS_2 were mechanically exfoliated from commercial bulk crystals (HQ Graphene) and vertically stacked onto the photonic crystal sample surface via dry transfer, forming a hybrid WS_2/hBN/grating heterostructure.

Optical Measurements. The momentum-space imaging was carried out by the homemade reflected momentum-space imaging spectroscopy based on the optical Fourier transformation method. The polarized incident light, regulated by a linear polarizer set at a specific angle, is focused onto the sample positioned in front of the objective lens (numerical aperture, NA = 0.5; manufactured by Olympus Company). Through the Fourier transform of the objective lens, the reflected light converges the momentum - related image in momentum space onto the back focal plane. The optical information on the back focal plane is projected onto the entrance slit of the spectrometer (iHR550, Horiba) via an achromatic doublet lens (4f optical system). Wavelength resolution is achieved by utilizing the blazed grating within the spectrometer. Finally, a liquid-nitrogen-cooled charge-coupled device (CCD) is employed to collect the information. For pump-dependent PL measurements were performed through real-space imaging of the device. An objective lens with a numerical aperture (NA) of 0.9 was employed for both focusing and collection. A continuous-wave solid-state laser (532 nm) with X polarization and a focused beam size of 2 μm was used to excite the monolayer WS_2. The resulting photoluminescence was then detected by a spectrometer (LabRAM HR Evolution, Horiba) with a cooled CCD (Symphony II, Horiba).

■ ASSOCIATED CONTENT

Supporting Information

The Supporting Information is available free of charge at https://pubs.acs.org/doi/10.1021/acs.nanolett.4c06464.

Additional information about quasinormal mode (QNM) method for calculating the plasmonic BIC, the electric field distribution in the plane, fabrication processes of the samples, the protective effect of hBN on strong coupling, coupled harmonic oscillator model, and schematic diagram of optical setups (PDF)

■ AUTHOR INFORMATION

Corresponding Authors

Yang Guo − *Beijing National Laboratory for Condensed Matter Physics, Institute of Physics, Chinese Academy of Sciences, Beijing 100190, China; School of Physical Sciences, CAS Key Laboratory of Vacuum Physics, University of Chinese Academy of Sciences, Beijing 100190, China;* orcid.org/0000-0001-8975-9387; Email: yangguo@iphy.ac.cn

Changzhi Gu − *Beijing National Laboratory for Condensed Matter Physics, Institute of Physics, Chinese Academy of Sciences, Beijing 100190, China; School of Physical Sciences, CAS Key Laboratory of Vacuum Physics, University of Chinese Academy of Sciences, Beijing 100190, China;* orcid.org/0000-0002-2689-2807; Email: czgu@iphy.ac.cn

Jianmei Li − *Key Laboratory for Microstructural Material Physics of Hebei Province, School of Science, Yanshan University, Qinhuangdao 066004, China;* orcid.org/0000-0002-5529-5251; Email: jianmeili@ysu.edu.cn

Authors

Cai Luo − *Beijing National Laboratory for Condensed Matter Physics, Institute of Physics, Chinese Academy of Sciences, Beijing 100190, China; Key Laboratory for Microstructural Material Physics of Hebei Province, School of Science, Yanshan University, Qinhuangdao 066004, China*

Wei Li − *Tsinghua Shenzhen International Graduate School, Tsinghua University, Shenzhen 518055, China;* orcid.org/0009-0003-8370-7705

Ziyi Fu − *Beijing National Laboratory for Condensed Matter Physics, Institute of Physics, Chinese Academy of Sciences, Beijing 100190, China; Key Laboratory for Microstructural Material Physics of Hebei Province, School of Science, Yanshan University, Qinhuangdao 066004, China*

Nannan Hu − *Beijing National Laboratory for Condensed Matter Physics, Institute of Physics, Chinese Academy of Sciences, Beijing 100190, China*

Zhixiang Yu − *Key Laboratory for Microstructural Material Physics of Hebei Province, School of Science, Yanshan University, Qinhuangdao 066004, China*

https://doi.org/10.1021/acs.nanolett.4c06464
Nano Lett. 2025, 25, 4361−4368

Wenyao Chang − *Beijing National Laboratory for Condensed Matter Physics, Institute of Physics, Chinese Academy of Sciences, Beijing 100190, China; Key Laboratory for Microstructural Material Physics of Hebei Province, School of Science, Yanshan University, Qinhuangdao 066004, China*
Pinxu Li − *Key Laboratory for Microstructural Material Physics of Hebei Province, School of Science, Yanshan University, Qinhuangdao 066004, China*
Xin Huang − *Beijing National Laboratory for Condensed Matter Physics, Institute of Physics, Chinese Academy of Sciences, Beijing 100190, China; School of Physical Sciences, CAS Key Laboratory of Vacuum Physics, University of Chinese Academy of Sciences, Beijing 100190, China*
Baoli Liu − *Beijing National Laboratory for Condensed Matter Physics, Institute of Physics, Chinese Academy of Sciences, Beijing 100190, China; School of Physical Sciences, CAS Key Laboratory of Vacuum Physics, University of Chinese Academy of Sciences, Beijing 100190, China*
Yang Yang − *Beijing National Laboratory for Condensed Matter Physics, Institute of Physics, Chinese Academy of Sciences, Beijing 100190, China;* orcid.org/0000-0003-3785-9233
Aizi Jin − *Beijing National Laboratory for Condensed Matter Physics, Institute of Physics, Chinese Academy of Sciences, Beijing 100190, China*
Baogang Quan − *Beijing National Laboratory for Condensed Matter Physics, Institute of Physics, Chinese Academy of Sciences, Beijing 100190, China; School of Physical Sciences, CAS Key Laboratory of Vacuum Physics, University of Chinese Academy of Sciences, Beijing 100190, China; Songshan Lake Material Laboratory, Dongguan, Guangdong 523808, China*
Shibing Tian − *Beijing National Laboratory for Condensed Matter Physics, Institute of Physics, Chinese Academy of Sciences, Beijing 100190, China*
Haifang Yang − *Beijing National Laboratory for Condensed Matter Physics, Institute of Physics, Chinese Academy of Sciences, Beijing 100190, China*

Complete contact information is available at: https://pubs.acs.org/10.1021/acs.nanolett.4c06464

Author Contributions

C.L. and W.L. contributed equally to this work. C.L., Y.G., and W.L. conceived the ideas and designed the experiments. C.L. prepared the monolayer microcavity samples. Y.G. and C.L. carried out the optical spectroscopy measurements. Y.G., W.L., J.L., and C.L. analyzed the data. Y.G., J.L., and C.L. wrote the manuscript with input from all authors.

Notes

The authors declare no competing financial interest.

■ ACKNOWLEDGMENTS

This work was supported by the National Key Research and Development Program of China under Grant Nos. 2024YFA1207700, 2022YFA1204100, 2021YFA1400700; National Natural Science Foundation of China under Grants Nos. 92265110, 62174179, 62204259; the Key Program of National Natural Science Foundation of China, Grant No. 12332002; Science Research Project of Hebei Education Department under Grant No. QN2024128; Strategic Priority Research Program of the Chinese Academy of Sciences under Grant No. XDB33020200; the CAS Project for Young Scientists in Basic Research (Grant No. YSBR-056). This work was also supported by the Micro/nano Fabrication Laboratory of Synergetic Extreme Condition User Facility (SECUF).

■ REFERENCES

(1) Sanvitto, D.; Kéna-Cohen, S. The road towards polaritonic devices. *Nat. Mater.* **2016**, *15* (10), 1061−1073.
(2) Deng, H.; Haug, H.; Yamamoto, Y. Exciton-polariton Bose−Einstein condensation. *Rev. Mod. Phys.* **2010**, *82* (2), 1489−1537.
(3) Kasprzak, J.; Richard, M.; Kundermann, S.; Baas, A.; Jeambrun, P.; Keeling, J. M. J.; Marchetti, F. M.; Szymańska, M. H.; André, R.; Staehli, J. L.; Savona, V.; Littlewood, P. B.; Deveaud, B.; Dang, L. S. Bose−Einstein condensation of exciton polaritons. *Nature* **2006**, *443* (7110), 409−414.
(4) Lerario, G.; Fieramosca, A.; Barachati, F.; Ballarini, D.; Daskalakis, K. S.; Dominici, L.; De Giorgi, M.; Maier, S. A.; Gigli, G.; Kéna-Cohen, S.; Sanvitto, D. Room-temperature superfluidity in a polariton condensate. *Nat. Phys.* **2017**, *13* (9), 837−841.
(5) Schneider, C.; Rahimi-Iman, A.; Kim, N. Y.; Fischer, J.; Savenko, I. G.; Amthor, M.; Lermer, M.; Wolf, A.; Worschech, L.; Kulakovskii, V. D.; Shelykh, I. A.; Kamp, M.; Reitzenstein, S.; Forchel, A.; Yamamoto, Y.; Höfling, S. An electrically pumped polariton laser. *Nature* **2013**, *497* (7449), 348−352.
(6) Lagoudakis, K. G.; Wouters, M.; Richard, M.; Baas, A.; Carusotto, I.; André, R.; Dang, L. S.; Deveaud-Plédran, B. Quantized vortices in an exciton−polariton condensate. *Nat. Phys.* **2008**, *4* (9), 706−710.
(7) Su, R.; Fieramosca, A.; Zhang, Q.; Nguyen, H. S.; Deleporte, E.; Chen, Z.; Sanvitto, D.; Liew, T. C. H.; Xiong, Q. Perovskite semiconductors for room-temperature exciton-polaritonics. *Nat. Mater.* **2021**, *20* (10), 1315−1324.
(8) Ghosh, S.; Su, R.; Zhao, J.; Fieramosca, A.; Wu, J.; Li, T.; Zhang, Q.; Li, F.; Chen, Z.; Liew, T.; Sanvitto, D.; Xiong, Q. Microcavity exciton polaritons at room temperature. *Photonics Insights* **2022**, *1* (1), R04.
(9) Ciuti, C.; Savona, V.; Piermarocchi, C.; Quattropani, A.; Schwendimann, P. Role of the exchange of carriers in elastic exciton-exciton scattering in quantum wells. *Phys. Rev. B* **1998**, *58* (12), 7926−7933.
(10) Kodigala, A.; Lepetit, T.; Gu, Q.; Bahari, B.; Fainman, Y.; Kanté, B. Lasing action from photonic bound states in continuum. *Nature* **2017**, *541* (7636), 196−199.
(11) Hsu, C. W.; Zhen, B.; Stone, A. D.; Joannopoulos, J. D.; Soljačić, M. Bound states in the continuum. *Nature Reviews Materials* **2016**, *1* (9), 16048.
(12) Liang, Y.; Tsai, D. P.; Kivshar, Y. From local to nonlocal high-Q plasmonic metasurfaces. *Phys. Rev. Lett.* **2024**, *133* (5), 053801.
(13) Lundt, N.; Klembt, S.; Cherotchenko, E.; Betzold, S.; Iff, O.; Nalitov, A. V.; Klaas, M.; Dietrich, C. P.; Kavokin, A. V.; Höfling, S.; Schneider, C. Room-temperature Tamm-plasmon exciton-polaritons with a WSe_2 monolayer. *Nat. Commun.* **2016**, *7* (1), 13328.
(14) Wang, S.; Li, S.; Chervy, T.; Shalabney, A.; Azzini, S.; Orgiu, E.; Hutchison, J. A.; Genet, C.; Samorì, P.; Ebbesen, T. W. Coherent coupling of WS_2 monolayers with metallic photonic nanostructures at room temperature. *Nano Lett.* **2016**, *16* (7), 4368−4374.
(15) Ballarini, D.; De Giorgi, M.; Cancellieri, E.; Houdré, R.; Giacobino, E.; Cingolani, R.; Bramati, A.; Gigli, G.; Sanvitto, D. All-optical polariton transistor. *Nat. Commun.* **2013**, *4* (1), 1778.
(16) Zhao, L.; Shang, Q.; Li, M.; Liang, Y.; Li, C.; Zhang, Q. Strong exciton-photon interaction and lasing of two-dimensional transition metal dichalcogenide semiconductors. *Nano Research* **2021**, *14* (6), 1937−1954.
(17) Liu, X.; Galfsky, T.; Sun, Z.; Xia, F.; Lin, E.-c.; Lee, Y.-H.; Kéna-Cohen, S.; Menon, V. M. Strong light−matter coupling in two-dimensional atomic crystals. *Nat. Photonics* **2015**, *9* (1), 30−34.
(18) Zhang, Q.; Shang, Q.; Su, R.; Do, T. T. H.; Xiong, Q. Halide perovskite semiconductor lasers: materials, cavity design, and low threshold. *Nano Lett.* **2021**, *21* (5), 1903−1914.

(19) Su, R.; Diederichs, C.; Wang, J.; Liew, T. C. H.; Zhao, J.; Liu, S.; Xu, W.; Chen, Z.; Xiong, Q. Room-temperature polariton lasing in all-inorganic perovskite nanoplatelets. *Nano Lett.* **2017**, *17* (6), 3982−3988.
(20) Chernikov, A.; Berkelbach, T. C.; Hill, H. M.; Rigosi, A.; Li, Y.; Aslan, B.; Reichman, D. R.; Hybertsen, M. S.; Heinz, T. F. Exciton binding energy and nonhydrogenic rydberg series in monolayer WS_2. *Phys. Rev. Lett.* **2014**, *113* (7), 076802.
(21) del Águila, A. G.; Wong, Y. R.; Wadgaonkar, I.; Fieramosca, A.; Liu, X.; Vaklinova, K.; Dal Forno, S.; Do, T. T. H.; Wei, H. Y.; Watanabe, K.; Taniguchi, T.; Novoselov, K. S.; Koperski, M.; Battiato, M.; Xiong, Q. Ultrafast exciton fluid flow in an atomically thin MoS_2 semiconductor. *Nat. Nanotechnol.* **2023**, *18* (9), 1012−1019.
(22) Cong, C.; Shang, J.; Wang, Y.; Yu, T. Optical properties of 2D semiconductor WS_2. *Advanced Optical Materials* **2018**, *6* (1), 1700767.
(23) Liu, X.; Bao, W.; Li, Q.; Ropp, C.; Wang, Y.; Zhang, X. Control of coherently coupled exciton polaritons in monolayer tungsten disulphide. *Phys. Rev. Lett.* **2017**, *119* (2), 027403.
(24) Qiu, L.; Chakraborty, C.; Dhara, S.; Vamivakas, A. N. Room-temperature valley coherence in a polaritonic system. *Nat. Commun.* **2019**, *10* (1), 1513.
(25) Lundt, N.; Dusanowski, Ł.; Sedov, E.; Stepanov, P.; Glazov, M. M.; Klembt, S.; Klaas, M.; Beierlein, J.; Qin, Y.; Tongay, S.; Richard, M.; Kavokin, A. V.; Höfling, S.; Schneider, C. Optical valley Hall effect for highly valley-coherent exciton-polaritons in an atomically thin semiconductor. *Nat. Nanotechnol.* **2019**, *14* (8), 770−775.
(26) Jiang, Y.; Wang, H.; Wen, S.; Chen, H.; Deng, S. Resonance coupling in an individual gold nanorod−monolayer WS_2 heterostructure: photoluminescence enhancement with spectral broadening. *ACS Nano* **2020**, *14* (10), 13841−13851.
(27) Kleemann, M.-E.; Chikkaraddy, R.; Alexeev, E. M.; Kos, D.; Carnegie, C.; Deacon, W.; de Pury, A. C.; Große, C.; de Nijs, B.; Mertens, J.; Tartakovskii, A. I.; Baumberg, J. J. Strong-coupling of WSe2 in ultra-compact plasmonic nanocavities at room temperature. *Nat. Commun.* **2017**, *8* (1), 1296.
(28) Wen, J.; Wang, H.; Wang, W.; Deng, Z.; Zhuang, C.; Zhang, Y.; Liu, F.; She, J.; Chen, J.; Chen, H.; Deng, S.; Xu, N. Room-Temperature Strong Light−Matter Interaction with Active Control in Single Plasmonic Nanorod Coupled with Two-Dimensional Atomic Crystals. *Nano Lett.* **2017**, *17* (8), 4689−4697.
(29) Yu, M.-W.; Ishii, S.; Li, S.; Ku, J.-R.; Yang, J.-H.; Su, K.-L.; Taniguchi, T.; Nagao, T.; Chen, K.-P. Quantifying photoinduced carriers transport in exciton−polariton coupling of MoS_2 monolayers. *npj 2D Materials and Applications* **2021**, *5* (1), 47.
(30) Zhang, M.; Tian, Y.; Chen, X.; Sun, Z.; Zhu, X.; Wu, J. Observation of ultra-large Rabi splitting in the plasmon-exciton polaritons at room temperature. *Nanophotonics* **2023**, *12* (16), 3267−3275.
(31) Yan, X.; Wei, H. Strong plasmon−exciton coupling between lithographically defined single metal nanoparticles and monolayer WSe_2. *Nanoscale* **2020**, *12* (17), 9708−9716.
(32) Liu, W.; Lee, B.; Naylor, C. H.; Ee, H.-S.; Park, J.; Johnson, A. T. C.; Agarwal, R. Strong exciton−plasmon coupling in MoS_2 coupled with plasmonic lattice. *Nano Lett.* **2016**, *16* (2), 1262−1269.
(33) Barachati, F.; Fieramosca, A.; Hafezian, S.; Gu, J.; Chakraborty, B.; Ballarini, D.; Martinu, L.; Menon, V.; Sanvitto, D.; Kéna-Cohen, S. Interacting polariton fluids in a monolayer of tungsten disulfide. *Nat. Nanotechnol.* **2018**, *13* (10), 906−909.
(34) Liu, W.; Ji, Z.; Wang, Y.; Modi, G.; Hwang, M.; Zheng, B.; Sorger, V. J.; Pan, A.; Agarwal, R. Generation of helical topological exciton-polaritons. *Science* **2020**, *370* (6516), 600−604.
(35) Zhang, L.; Gogna, R.; Burg, W.; Tutuc, E.; Deng, H. Photonic-crystal exciton-polaritons in monolayer semiconductors. *Nat. Commun.* **2018**, *9* (1), 713.
(36) Paik, E. Y.; Zhang, L.; Hou, S.; Zhao, H.; Chou, Y.-H.; Forrest, S. R.; Deng, H. High quality factor microcavity for van der waals semiconductor polaritons using a transferrable mirror. *Advanced Optical Materials* **2023**, *11* (1), 2201440.
(37) Schneider, C.; Glazov, M. M.; Korn, T.; Höfling, S.; Urbaszek, B. Two-dimensional semiconductors in the regime of strong light-matter coupling. *Nat. Commun.* **2018**, *9* (1), 2695.
(38) Wu, T.; Wang, C.; Hu, G.; Wang, Z.; Zhao, J.; Wang, Z.; Chaykun, K.; Liu, L.; Chen, M.; Li, D.; Zhu, S.; Xiong, Q.; Shen, Z.; Gao, H.; Garcia-Vidal, F. J.; Wei, L.; Wang, Q. J.; Luo, Y. Ultrastrong exciton-plasmon couplings in WS_2 multilayers synthesized with a random multi-singular metasurface at room temperature. *Nat. Commun.* **2024**, *15* (1), 3295.
(39) Stührenberg, M.; Munkhbat, B.; Baranov, D. G.; Cuadra, J.; Yankovich, A. B.; Antosiewicz, T. J.; Olsson, E.; Shegai, T. Strong light−matter coupling between plasmons in individual gold bi-pyramids and excitons in mono- and multilayer WSe_2. *Nano Lett.* **2018**, *18* (9), 5938−5945.
(40) Zheng, D.; Zhang, S.; Deng, Q.; Kang, M.; Nordlander, P.; Xu, H. Manipulating coherent plasmon−exciton interaction in a single silver nanorod on monolayer WSe_2. *Nano Lett.* **2017**, *17* (6), 3809−3814.
(41) Xie, P.; Liang, Z.; Jia, T.; Li, D.; Chen, Y.; Chang, P.; Zhang, H.; Wang, W. Strong coupling between excitons in a two-dimensional atomic crystal and quasibound states in the continuum in a two-dimensional all-dielectric asymmetric metasurface. *Phys. Rev. B* **2021**, *104* (12), 125446.
(42) Gogna, R.; Zhang, L.; Wang, Z.; Deng, H. Photonic crystals for controlling strong coupling in van der Waals materials. *Opt. Express* **2019**, *27* (16), 22700−22707.
(43) Sun, S.; Ding, Y.; Li, H.; Hu, P.; Cheng, C.-W.; Sang, Y.; Cao, F.; Hu, Y.; Alù, A.; Liu, D.; Wang, Z.; Gwo, S.; Han, D.; Shi, J. Tunable plasmonic bound states in the continuum in the visible range. *Phys. Rev. B* **2021**, *103* (4), 045416.
(44) Hsu, C. W.; Zhen, B.; Lee, J.; Chua, S.-L.; Johnson, S. G.; Joannopoulos, J. D.; Soljačić, M. Observation of trapped light within the radiation continuum. *Nature* **2013**, *499* (7457), 188−191.
(45) Huang, S.; Ming, T.; Lin, Y.; Ling, X.; Ruan, Q.; Palacios, T.; Wang, J.; Dresselhaus, M.; Kong, J. Ultrasmall mode volumes in plasmonic cavities of nanoparticle on mirror structures. *Small* **2016**, *12* (37), 5190−5199.
(46) Berkdemir, A.; Gutiérrez, H. R.; Botello-Méndez, A. R.; Perea-López, N.; Elías, A. L.; Chia, C.-I.; Wang, B.; Crespi, V. H.; López-Urías, F.; Charlier, J.-C.; Terrones, H.; Terrones, M. Identification of individual and few layers of WS_2 using Raman spectroscopy. *Sci. Rep.* **2013**, *3* (1), 1755.
(47) Molas, M. R.; Nogajewski, K.; Potemski, M.; Babiński, A. Raman scattering excitation spectroscopy of monolayer WS_2. *Sci. Rep.* **2017**, *7* (1), 5036.
(48) Knobloch, T.; Illarionov, Y. Y.; Ducry, F.; Schleich, C.; Wachter, S.; Watanabe, K.; Taniguchi, T.; Mueller, T.; Waltl, M.; Lanza, M.; Vexler, M. I.; Luisier, M.; Grasser, T. The performance limits of hexagonal boron nitride as an insulator for scaled CMOS devices based on two-dimensional materials. *Nature Electronics* **2021**, *4* (2), 98−108.
(49) Fukamachi, S.; Solís-Fernández, P.; Kawahara, K.; Tanaka, D.; Otake, T.; Lin, Y.-C.; Suenaga, K.; Ago, H. Large-area synthesis and transfer of multilayer hexagonal boron nitride for enhanced graphene device arrays. *Nature Electronics* **2023**, *6* (2), 126−136.
(50) Zhang, Y.; Chen, A.; Liu, W.; Hsu, C. W.; Wang, B.; Guan, F.; Liu, X.; Shi, L.; Lu, L.; Zi, J. Observation of polarization vortices in momentum space. *Phys. Rev. Lett.* **2018**, *120* (18), 186103.
(51) Hopfield, J. J. Theory of the contribution of excitons to the complex dielectric constant of crystals. *Phys. Rev.* **1958**, *112* (5), 1555−1567.
(52) Zhong, J.; Li, J.-Y.; Liu, J.; Xiang, Y.; Feng, H.; Liu, R.; Li, W.; Wang, X.-H. Room-temperature strong coupling of few-exciton in a monolayer WS_2 with plasmon and dispersion deviation. *Nano Lett.* **2024**, *24* (5), 1579−1586.

https://doi.org/10.1021/acs.nanolett.4c06464
Nano Lett. 2025, 25, 4361−4368